Intracellular collagen degradation mediated by uPARAP/Endo180 is a major pathway of extracellular matrix turnover during malignancy

Alejandro C. Curino,[1] Lars H. Engelholm,[4] Susan S. Yamada,[3] Kenn Holmbeck,[3] Leif R. Lund,[4] Alfredo A. Molinolo,[2] Niels Behrendt,[4] Boye Schnack Nielsen,[4] and Thomas H. Bugge[1]

[1]Proteases and Tissue Remodeling Unit and [2]Molecular Carcinogenesis Unit, Oral and Pharyngeal Cancer Branch, and [3]Matrix Metalloproteinase Unit, Craniofacial and Skeletal Diseases Branch, National Institute of Dental and Craniofacial Research, National Institutes of Health, Bethesda, MD 20892
[4]Finsen Laboratory, Rigshospitalet, DK-2100 Copenhagen Ø, Denmark

We recently reported that uPARAP/Endo180 can mediate the cellular uptake and lysosomal degradation of collagen by cultured fibroblasts. Here, we show that uPARAP/Endo180 has a key role in the degradation of collagen during mammary carcinoma progression. In the normal murine mammary gland, uPARAP/Endo180 is widely expressed in periductal fibroblast-like mesenchymal cells that line mammary epithelial cells. This pattern of uPARAP/Endo180 expression is preserved during polyomavirus middle T–induced mammary carcinogenesis, with strong uPARAP/Endo180 expression by mesenchymal cells embedded within the collagenous stroma surrounding nests of uPARAP/Endo180-negative tumor cells. Genetic ablation of uPARAP/Endo180 impaired collagen turnover that is critical to tumor expansion, as evidenced by the abrogation of cellular collagen uptake, tumor fibrosis, and blunted tumor growth. These studies identify uPARAP/Endo180 as a key mediator of collagen turnover in a pathophysiological context.

Introduction

Malignant progression is an example of a radical tissue remodeling process in which one tissue (normal tissue) is invaded and is eventually completely substituted by a different tissue (tumor tissue). The process is characterized by dramatic increases in both the rate of synthesis and the rate of turnover of ECM components in a complex cycle of continuous ECM deposition and degradation. ECM degradation serves at least four different functions that all are essential to tumor progression. It facilitates the physical expansion of the tumor mass, liberates latent tumor growth factors embedded within the ECM, enables the formation of a neovasculature within the expanding tumor mass, and subverts the proliferative restrictions imposed on tumor cells by ECM (Hotary et al., 2003; Mott and Werb, 2004). Inhibition of ECM degradation has, therefore, long been recognized as an attractive target for therapeutic intervention aimed at limiting tumor growth (Coussens and Werb, 2002).

The degradation of ECM during malignant progression is a proteolytic event. Because most tumor cell lines produce increased levels of proteases, ECM degradation was initially believed to be a relatively simple process that was executed directly by tumor cells through the secretion of an assortment of ECM-degrading proteases (Liotta et al., 1980, 1991; Danø et al., 1985). However, an exhaustive body of work that now spans more than two decades has demonstrated a much higher level of complexity. Thus, the current paradigm holds that ECM degradation during malignant progression is the result of a finely coordinated interplay between tumor cells, tumor-associated stromal cells, and tumor-infiltrating inflammatory cells, each having distinct and indispensable roles in the process. Furthermore, this work has identified the tumor stromal cell as one of the principle mediators of ECM turnover during tumor invasion. As such, malignant progression may show striking similarities to a variety of normal physiological tissue remodeling processes (Danø et al., 1999; Werb et al., 1999; Liotta and Kohn, 2001).

Collagens are the most abundant ECM components in the body and are a universal part of the tumor ECM (Hanahan and Weinberg, 2000; Liotta and Kohn, 2001; Chambers et al., 2002). They consist of three polypeptide chains, each with a single, long uninterrupted section of Gly-X-Y repeats that are intertwined to produce a superhelix that buries the peptide bonds within the interior of the helix. The fibrillar collagens spontaneously self associate to form fibrils that range in diameter

Correspondence to Thomas H. Bugge: thomas.bugge@nih.gov
Abbreviation used in this paper: PymT; polyomavirus middle T.

The Journal of Cell Biology, Vol. 169, No. 6, June 20, 2005 977–985
http://www.jcb.org/cgi/doi/10.1083/jcb.200411153

from 10 to 300 nm, whereas basement membrane collagens form complicated sheets with both triple helical and globular motifs (van der Rest and Garrone, 1991). The unique supramolecular organization makes fibrillar collagens relatively resistant to proteolytic degradation. However, several molecular pathways that are involved in the turnover of collagen in normal physiological processes have been identified. One pathway involves a group of secreted or membrane-associated matrix metalloproteases (collagenases) and is believed to take place within the pericellular/extracellular environment. A second cathepsin-mediated pathway that is specific for bone resorption takes place in the acidic microenvironment that is created at the osteoclast/osteoid interface (Gelb et al., 1996; Saftig et al., 1998). A third pathway is intracellular and involves the binding of collagen fibrils to specific cell surface receptors, followed by the cellular uptake and proteolytic degradation of internalized collagen in the lysosomal compartment (Everts et al., 1996). The contributions of pericellular/extracellular proteolytic pathways to collagen degradation during tumor progression are documented in numerous studies (Mott and Werb, 2004). In sharp contrast, the functional involvement of the intracellular collagen degradation pathway to this important pathophysiological process is unexplored to date.

uPARAP/Endo180 is a newly discovered member of the macrophage mannose receptor family of endocytic transmembrane glycoproteins. The receptor is highly expressed by certain mesenchymal cells that are located at sites of active tissue remodeling, including human cancer (Schnack Nielsen et al., 2002). By gene targeting in mice, we recently identified a critical role of uPARAP/Endo180 in the cellular uptake and lysosomal degradation of collagen (Engelholm et al., 2003; Kjøller et al., 2004). We now have taken advantage of the availability of these mutant mice with a defect in intracellular collagen degradation to determine the functional contribution of this pathway to collagen turnover in cancer by using a validated murine model of ductal mammary adenocarcinoma (Guy et al., 1992; Maglione et al., 2001; Lin et al., 2003). We report that intracellular collagen degradation by tumor stromal cells is a functionally relevant pathway for collagen turnover during malignant progression, and this process is meditated by uPARAP/Endo180. This finding has important implications for the understanding of ECM turnover in cancer.

Results

uPARAP/Endo180 expression in polyomavirus middle T (PymT)–induced mammary adenocarcinoma mimics expression in human mammary cancer

We have previously shown that uPARAP/Endo180 expression is limited in the normal human mammary gland, but the receptor becomes highly expressed by mesenchymal stromal cells during mammary tumorigenesis (Schnack Nielsen et al., 2002). To determine if the expression of uPARAP/Endo180 in PymT-induced ductal mammary adenocarcinoma resembles the expression pattern observed in the human disease, we first performed an immunohistochemical analysis of the normal murine mammary gland and PymT-induced mammary tumors. As a control for antibody specificity, we included uPARAP/Endo180-deficient mammary glands and tumors in the analysis. uPARAP/Endo180 expression in the resting virgin mouse mammary gland was detected in fibroblast-like cells lining the periphery of mammary ducts, in connective tissue trabeculae encapsulating the gland, and dispersed within adipose tissue (Fig. 1 A and not depicted). This expression pattern was faithfully maintained throughout PymT-induced mammary tumor progression, with strong uPARAP/Endo180 immunoreactivity in fibroblast-like cells embedded within the collagenous stroma surrounding or adjacent to nests of tumor cells (Fig. 1, B and C). Like human mammary cancer, the tumor cells were uPARAP/Endo180-negative at all analyzed stages (Fig. 1, B and C). The identical pattern of expression of uPARAP/Endo180 mRNA in normal and malignant mammary glands was observed by in situ hybridization (Fig. 1, E and F; and not depicted). Together, these data show that uPARAP/Endo180 expression during PymT-induced mammary carcinogenesis in mice resembles the previously established pattern of expression in the human mammary gland and human mammary cancer and validates the PymT model as suitable for functional studies of uPARAP/Endo180.

uPARAP/Endo180 mediates collagen uptake and degradation by tumor stromal cells during mammary tumor progression

To determine the functional relevance of stromal uPARAP/Endo180 in mammary cancer, we took advantage of the availability of recently generated uPARAP/Endo180-deficient mice. These mice are viable and fertile and display good health in the absence of external challenges or additional genetic defects in collagenolytic pathways (Engelholm et al., 2003). The uPARAP/Endo180-deficient mice were first extensively backcrossed to FVB mice and were subsequently interbred with FVB-PymT mice to generate mice that developed mammary tumors in the presence and absence of uPARAP/Endo180. To study cellular collagen turnover within PymT-induced mammary tumors, we first explanted uPARAP/Endo180-sufficient and -deficient tumors ex vivo by using a modification of previously established procedures that allow the short term coculture of mammary tumor cells with their associated tumor stromal cells (Pandis et al., 1992; Dran et al., 1995; Lanari et al., 2001). The explants spontaneously organized as epithelial sheets of tightly clustered tumor cells that were surrounded by larger mesenchymal cells with a typical fibroblast morphology (Fig. 2 A). Oregon green–conjugated collagen fibrils were added to the explants, and the fate of the labeled collagen was studied by confocal fluorescence microscopy in the presence of the cysteine protease inhibitor E64d, which blocks lysosomal degradation of collagen (Kjøller et al., 2004). 8 h after the addition of collagen, the majority of labeled collagen was located within vesicular structures of the stromal cells of uPARAP/Endo180-sufficient explants (Fig. 2 B). Confocal fluorescence microscopy analysis showed that a subset of these collagen-containing vesicles of predominantly perinuclear localization were also

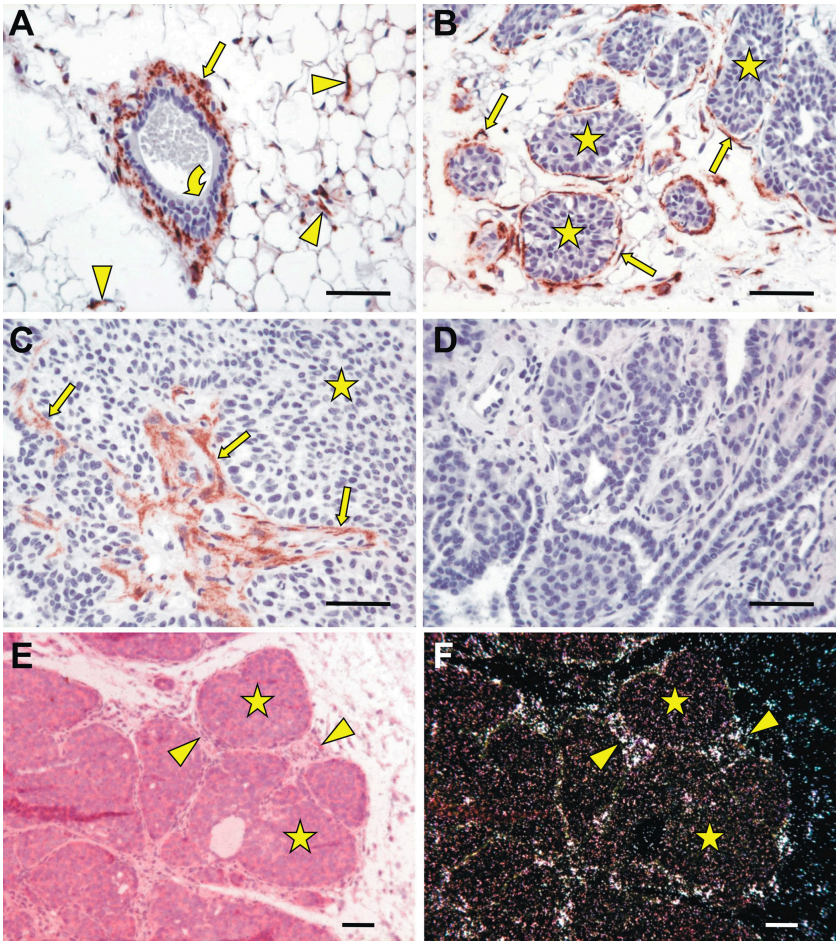

Figure 1. **uPARAP/Endo180 is expressed in fibroblast-like stromal cells of the normal murine mammary gland and mammary tumors.** (A) Immunohistochemical staining of normal virgin mammary gland showing expression of uPARAP/Endo180 in fibroblast-like mesenchymal cells lining the periphery of mammary ducts (arrow) and fibroblast-like cells embedded in adipose tissue (arrowheads), but not in mammary epithelial cells (curved arrow). (B) Mammary intraepithelial neoplasia in a 5-wk-old PymT female mouse showing periductal expression of uPARAP/Endo180 in fibroblast-like mesenchymal cells (arrows), but absence of uPARAP/Endo180 expression in mammary tumor cells (stars). (C) Advanced mammary carcinoma in a 13-wk-old PymT mouse showing uPARAP/Endo180 expression in fibroblast-like cells in connective tissue streaks transecting tumors (arrows), and absence of uPARAP/Endo180 expression in mammary tumor cells (star). (D) Absence of immunoreactivity in a tumor from a 13-wk-old PymT/uPARAP/Endo180$^{-/-}$ mouse stained in parallel demonstrates the specificity of the immunostaining procedure for uPARAP/Endo180. Brightfield (E) and darkfield (F) images of in situ hybridization using a uPARAP antisense probe of a mammary tumor from a 15-wk-old mouse, demonstrating the identical distribution of uPARAP/Endo180 mRNA and antigen, with uPARAP/Endo180 mRNA in stromal cells (arrowheads) adjacent to nests of uPARAP/Endo180 mRNA-negative tumor cells (stars). Bars, 50 μm.

stained with LysoTracker, a specific marker for lysosomes, suggesting that collagen was targeted for lysosomal degradation after the initial uptake by tumor stromal cells (Fig. 2 B). This cellular association was exclusively confined to the stromal fibroblast-like cells, with no tumor cell–associated collagen being apparent, as judged by visualization of the tumor cells with cytokeratin antibodies (Fig. 2 D). In striking contrast, in uPARAP/Endo180-deficient tumor explants, the collagen remained extracellular and formed fiberlike structures that were located in close proximity to the stromal cells (Fig. 2 C). To study collagen internalization in uPARAP/Endo180-sufficient and -deficient explants in greater detail, a time course study was used. Oregon green–conjugated collagen fibrils were added to the explants at 4°C to permit cell surface binding but not internalization of the collagen, and, thereafter, unbound collagen was removed by washing. At this time point, confocal analysis showed a mostly diffuse localization of the labeled collagen and occasionally showed poorly organized fiberlike structures (Fig. 2, E and F). A similar distribution has been described after the addition of collagen fibrils to cultured dermal fibroblasts at 4°C (Kjøller et al., 2004). Collagen internalization was initiated by raising the temperature of the explants to 37°C. After 2 h, the labeled collagen was associated with the surface of cells in explants from both genotypes, with small amounts of collagen appearing in intracellular vesicles of uPARAP/Endo180-sufficient (Fig. 2 G), but not uPARAP/Endo180-deficient, explants (Fig. 2 H). After 4 h, most of the collagen that was added to uPARAP/Endo180-sufficient explants was located in intracellular vesicles, frequently located in lysosomes (as judged by colocalization with LysoTracker), with smaller amounts in fiberlike extracellular structures (Fig. 2 I). At this time point, collagen remained in extracellular fiberlike structures of uPARAP/Endo180-deficient explants, generally displaying a greater organization compared with 2 h after the temperature shift (Fig. 2 J). Altogether, the data show that tumor stromal cells mediate the time-dependent cellular uptake and intracellular degradation of collagen in primary mammary tumor explants and that this process is strictly uPARAP/Endo180 dependent.

Next, the uPARAP/Endo180-dependent cellular uptake of collagen by PymT-induced mammary tumors was analyzed by transmission electron microscopy of uPARAP/Endo180-deficient and -sufficient tumors that were excised directly from 95–105-d-old mice. In uPARAP/Endo180-sufficient tumors, prominent intracellular membrane–bordered collagen inclusions were present in cells with an ultrastructural morphology compatible with fibroblasts. The intracellular collagen presented as transected bundles of fibrils or longitudinally dissected fibrils with typical periodicity, often located close to the nucleus (Fig. 2 K and not depicted). These collagen inclusions were morphologically similar to phagocytosed collagen inclusions, which were described previously in fibroblasts associ-

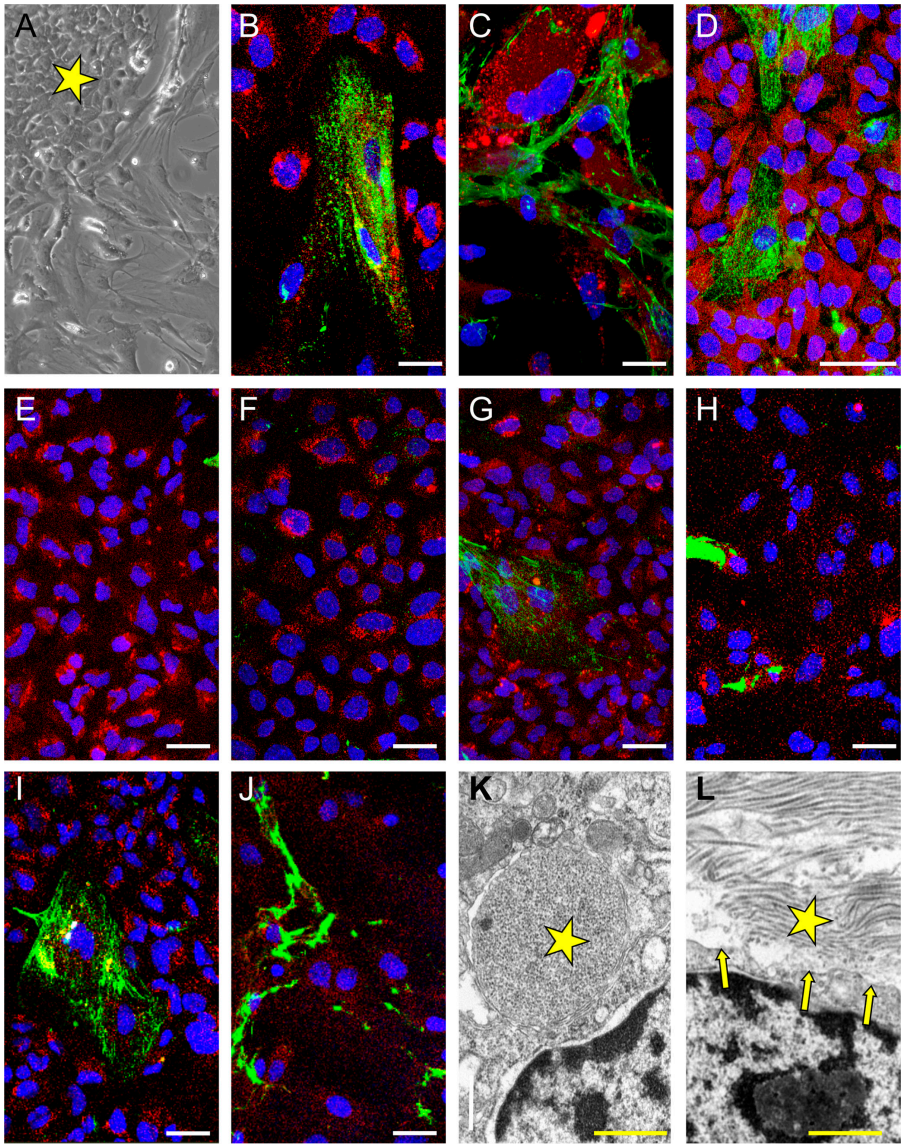

Figure 2. **uPARAP/Endo180 mediates cellular collagen uptake in mammary tumors.** (A) Phase-contrast micrograph of explanted uPARAP/Endo180^{+} mammary tumors showing spontaneous organization of tightly clustered sheets of small epithelial tumor cells (star) surrounded by larger mesenchymal cells with a typical fibroblast morphology. (B and C) Representative confocal fluorescence images of explants of mammary tumors from uPARAP/Endo180^{+} (B) and littermate uPARAP/Endo180$^{-/-}$ (C) mice 8 h after the addition of Oregon green–conjugated collagen fibrils to the explant medium. Explants were stained with LysoTracker (red) for the visualization of lysosomes and DAPI (blue) for the visualization of nuclei. uPARAP/Endo180^{+} tumor explants display the uptake of fluorescence-labeled collagen (green) into vesicles of large mesenchymal, fibroblast-like stromal cells located adjacent to mammary tumor cell clusters. Targeting of collagen to lysosomes is shown by the colocalization of green and red fluorescence (B, yellow) in some perinuclear vesicles. In sharp contrast to uPARAP/Endo180^{+} explants, collagen deposits in extracellular fiberlike structures in uPARAP/Endo180$^{-/-}$ mammary tumor explants. (D) Confocal fluorescence images after labeling of tumor cells with cytokeratin antibodies (red) shows the absence of internalized collagen in tumor cells. (E–J) Time course analysis of collagen internalization in uPARAP/Endo180^{+} (E, G, and I) and uPARAP/Endo180$^{-/-}$ explants (F, H, and J) using Oregon green–conjugated collagen fibrils and LysoTracker for visualization of lysosomes. Diffuse localization of collagen with occasional fiberlike structures immediately after collagen addition (E and F). Increased cellular association after 2 h, with some collagen in intracellular vesicles in uPARAP/Endo180^{+} explants (G), but not in uPARAP/Endo180$^{-/-}$ explants (H). (I) Predominant localization of collagen in intracellular vesicles of stromal cells of uPARAP/Endo180^{+} explants at 4 h, frequently colocalizing with LysoTracker-positive vesicles with perinuclear locations, versus the location of collagen in extracellular fiberlike structures with an increasing degree of organization compared with those after 2 h in uPARAP/Endo180$^{-/-}$ explants (J). (K and L) Representative examples of high magnification transmission electron micrographs of mammary tumor stromal cells from 105-d-old mice showing intracellular collagen inclusion (star) that is adjacent to the nucleus of a uPARAP/Endo180^{+} fibroblast (K) and the exclusively extracellular localization of collagen (star) in uPARAP/Endo180$^{-/-}$ tumors (L). Arrows (L) show the position of the plasma membrane. Bars: (B–J) 40 μm; (K and L) 500 nm.

ated with rheumatoid arthritis in humans or experimentally induced polyarthritis in rats and in lung macrophages during experimental emphysema (Cullen, 1972; Neurath, 1993; Lucattelli et al., 2003). In striking contrast, a survey of 56 sections from three uPARAP/Endo180-deficient tumors showed absence of intracellular collagen (Fig. 2 L). When combined, the data support the notion that the cellular uptake of collagen in mammary tumors is mediated by a uPARAP/Endo180-dependent pathway.

uPARAP/Endo180 deficiency initiates mammary tumor fibrosis

The contribution of stromal uPARAP/Endo180 to collagen turnover during mammary tumor progression was determined by analyzing collagen accumulation in mammary tumors from uPARAP/Endo180-deficient FVB-PymT^{+} virgin females and isogenic uPARAP/Endo180-sufficient FVB-PymT^{+} virgin female littermates. Immunohistochemical staining of tumors from 105-d-old mice revealed a striking increase in both interstitial (type I) and basement (type IV) collagen in uPARAP/Endo180-deficient animals, which was immediately evident by microscopic inspection (Fig. 3, A–D) and could be quantitatively documented by histomorphometric analysis (Fig. 3 K). In contrast, fibronectin (Fig. 3, E and F), which is internalized by mesenchymal cells in a uPARAP/Endo180-independent manner (Engelholm et al., 2003), and the collagen-associated ECM proteins decorin (Fig. 3, G and H) and nidogen (Fig. 3, I and J) did not display significantly increased accumulation in uPARAP/Endo180-deficient tumors. The significant increase in tumor collagen was not caused by an increase in collagen synthesis, as shown by Northern blot analysis of collagen Col1A1 and Col4A1 mRNA (Fig. 3 L) or immunohistochemical

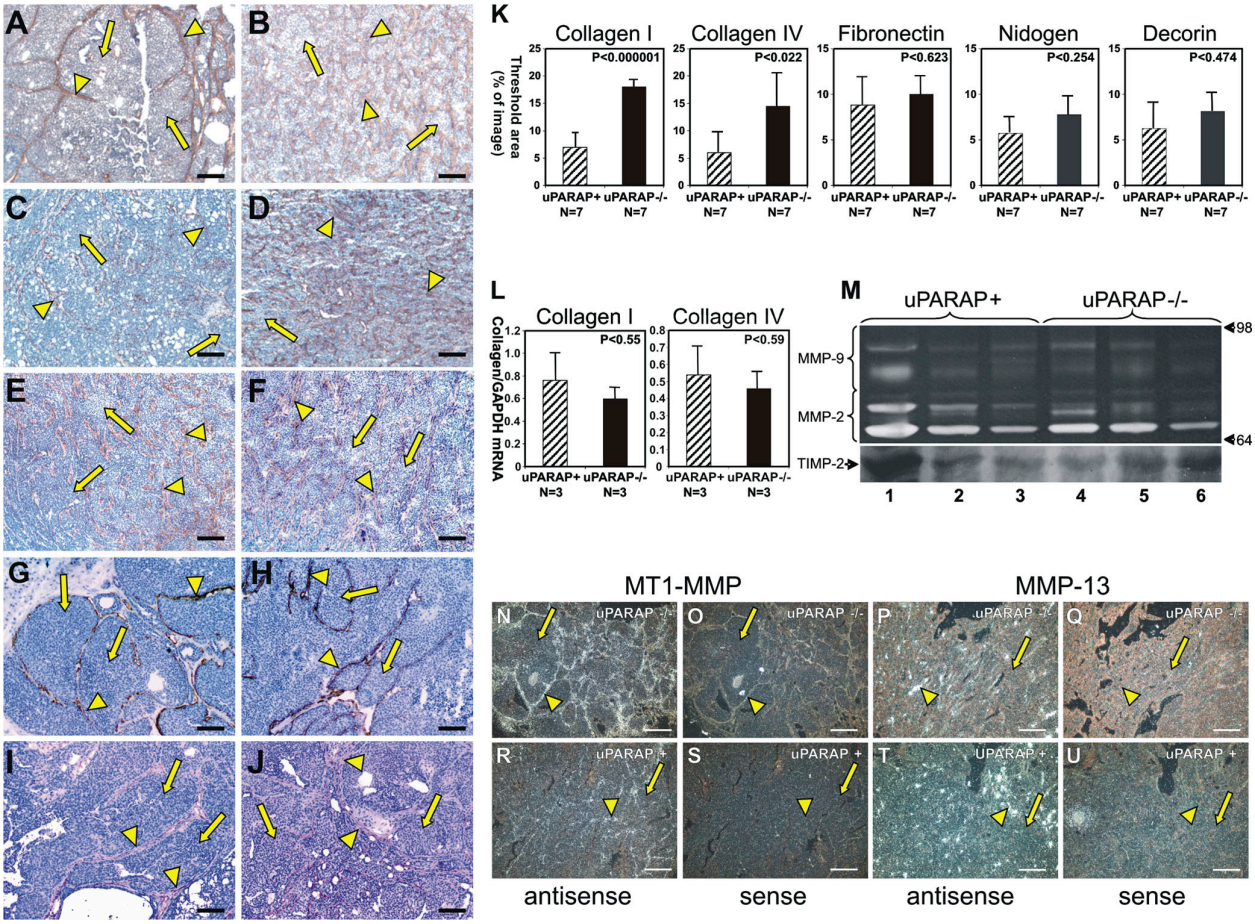

Figure 3. **Collagen accumulation in uPARAP/Endo180-deficient mammary tumors.** Representative examples of the appearance of uPARAP/Endo180^{+} tumors (A, C, E, G, and I) and uPARAP/Endo180$^{-/-}$ tumors (B, D, F, H, and J) after immunohistochemical staining for collagen type I (A and B), type IV (C and D), fibronectin (E and F), decorin, (G and H), and nidogen (I and J). uPARAP/Endo180$^{-/-}$ tumors display an obvious accumulation of collagen in the tumor stroma (arrowheads) surrounding nests of tumor cells (A–D, arrows), whereas no significant changes are apparent in fibronectin, nidogen, or decorin deposition (arrowheads) around tumor cell nests (E–J, arrows). (K) Histomorphometric quantitation of collagen I, collagen IV, fibronectin, nidogen, and decorin accumulation in uPARAP/Endo180^{+} (crosshatched bars) and uPARAP/Endo180$^{-/-}$ (shaded bars) tumors. (L) Northern blot analysis of Col1A1 and Col4A1 mRNA in uPARAP/Endo180^{+} (crosshatched bars) and uPARAP/Endo180$^{-/-}$ (shaded bars) tumors. Signal intensities were determined by PhosphorImage analysis and normalized to the GAPDH mRNA signal intensity. Error bars indicate SEM. (M) Gelatin zymography (top) of extracts of uPARAP/Endo180^{+} (lanes 1–3) and uPARAP/Endo180$^{-/-}$ tumors (lanes 4–6), and reverse zymography (bottom) showing amounts of zymographically active MMP-2, MMP-9, and TIMP-2. The position of lysis zones generated by MMP-2 and active MMP-9 and zones of inhibition of lysis by TIMP-2 are indicated at left. The positions of molecular mass markers (kD) are indicated at right. (N–U) Representative examples of in situ hybridization of MT1-MMP (N, O, R, and S) and MMP-13 (P, Q, T, and U) mRNA expression in uPARAP/Endo180$^{-/-}$ tumors (N–Q) and uPARAP/Endo180^{+} tumors (R–U) using ^{32}P-labeled antisense probes and complementary sense probes. Specific hybridization signals in uPARAP/Endo180-sufficient and -deficient tumors are observed in stromal cells (arrowheads) surrounding nests of tumor cells (arrows). Six tumors were analyzed for each of the two MMPs. Bars: (A–J) 500 μm; (N–U) 100 μm. All p-values were determined by a two-tailed *t* test.

staining with collagen I propeptide antibodies (not depicted). Gelatin zymography (Fig. 3 M, top) and reverse zymography (Fig. 3 M, bottom) showed abundant and variable levels of collagenase/gelatinase, MMP-2, gelatinase, MMP-9, and TIMP-2, which did not correlate with the uPARAP/Endo180 status. Likewise, uPARAP/Endo180 deficiency did not alter the expression of the collagenases MT1-MMP and MMP-13 (Fig. 3, N–U). Altogether, these findings point to a direct and quantitatively relevant role of uPARAP/Endo180 in mediating cellular uptake and lysosomal degradation of collagen during mammary tumor progression. Besides fibroblasts, uPARAP/Endo180 has been reported to be expressed on tumor endothelial cells and macrophages, invoking a potential function of the receptor for the functionality of the two cell types within the tumor environment (Sheikh et al., 2000; St Croix et al., 2000). However, uPARAP/Endo180 deficiency did not appear to impair either tumor vascularization, as judged by the density of CD31-positive vessels, or macrophage accumulation, as judged by the number of F4/80-positive cells (vessels per 100 cells: uPARAP/Endo180^{+}/PymT^{+}, 4.0 ± 0.6 [n = 5 tumors]; uPARAP/Endo180$^{-/-}$/PymT^{+}, 3.7 ± 0.3 [n = 5 tumors], P = NS. Macrophages per 100 cells: uPARAP/Endo180^{+}/PymT^{+}, 1.6 ± 0.3 [n = 5 tumors]; uPARAP/Endo180$^{-/-}$/PymT^{+}, 2.0 ± 0.6 [n = 5 tumors], P = NS).

A recent study has implicated the rate of turnover of three-dimensional collagen matrices as a critical regulator of tumor cell proliferation (Hotary et al., 2003). To determine the effect of increased collagen deposition caused by uPARAP/

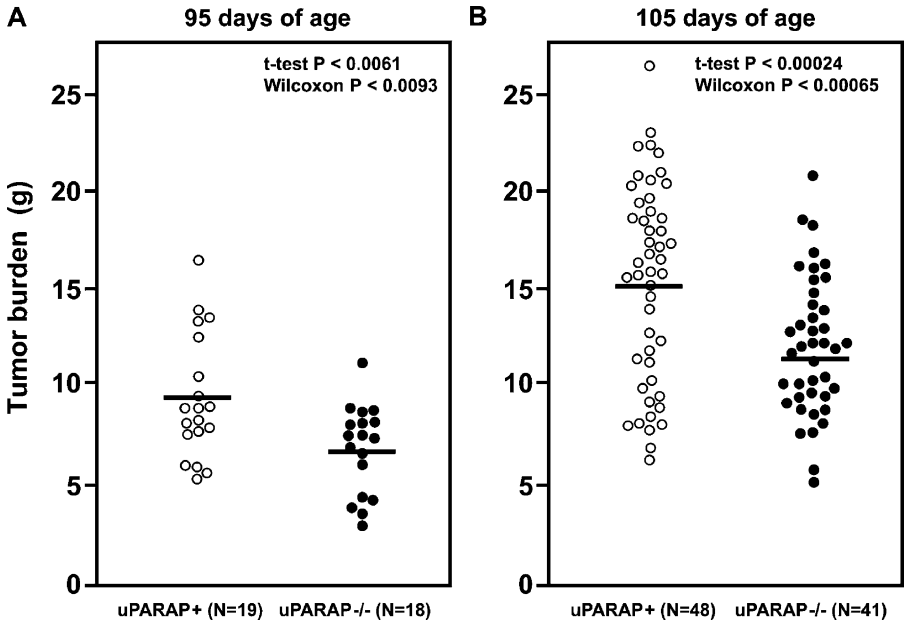

Figure 4. **uPARAP/Endo180 promotes mammary tumor progression.** Scatter plots of the cumulative tumor burdens of uPARAP/Endo180^{+} (open circles) and uPARAP/Endo180$^{-/-}$ (filled circles) mice at 95 (A) and 105 d of age (B), as determined by postmortem measurement of the weight of excised mammary tumors. Horizontal bars indicate mean values. P-values determined by a two-tailed *t* test and a Wilcoxon rank sum test are shown. N indicates the number of mice analyzed.

Endo180 deficiency on tumor cell proliferation, proliferative indices of uPARAP/Endo180-deficient and -sufficient tumors were determined by BrdU incorporation. This experiment showed no appreciable difference in the rate of proliferation of uPARAP/Endo180-sufficient and -deficient tumors, suggesting that the increased accumulation of collagen in uPARAP/Endo180-deficient tumors does not significantly impair tumor cell proliferation (percentage of BrdU-incorporating cells: uPARAP/Endo180^{+}/PymT^{+}, 6.5 ± 2.4 [n = 5 tumors]; uPARAP/Endo180$^{-/-}$/PymT^{+}, 6.6 ± 2.7 [n = 5 tumors], P = NS). Furthermore, we also did not observe a trend toward an increased rate of tumor cell apoptosis, as measured by TUNEL staining (percentage of apoptotic cells: uPARAP/Endo180^{+}/PymT^{+}, 0.7 ± 0.3 [n = 3 tumors]; uPARAP/Endo180$^{-/-}$/PymT^{+}, 0.8 ± 0.2 [n = 3 tumors], P = NS).

uPARAP/Endo180 promotes mammary tumor growth

We next determined the direct impact of the loss of uPARAP/Endo180 on mammary tumor growth. For this purpose, cohorts of uPARAP/Endo180-deficient FVB-PymT^{+} virgin females and isogenic uPARAP/Endo180-sufficient FVB-PymT^{+} virgin female littermates and siblings were generated and monitored for mammary tumor development. No differences were observed in the initial rate of formation of palpable mammary tumors or in the mean number of tumors that formed in the mice, showing that uPARAP/Endo180 is not essential for tumorigenesis (mean tumor latency: uPARAP/Endo180$^{-/-}$/PymT^{+}, 48 d [n = 47 mice]; uPARAP/Endo180^{+}/PymT^{+}, 47 d [n = 48 mice], P = NS. All of the 49 uPARAP/Endo180^{+} and 41 uPARAP/Endo180$^{-/-}$ mice had tumors in all mammary glands at 105 d). Interestingly, however, despite the prominent accumulation of collagen in the uPARAP/Endo180-deficient tumors, the size of the tumors was significantly diminished rather than increased (Fig. 4). This diminution of tumor growth in uPARAP/Endo180-deficient tumors was evident at both 95 (Fig. 4 A) and 105 d of age (Fig. 4 B), as determined by the accumulated tumor burden of postmortem excised tumors from two independent cohorts of littermate uPARAP/Endo180-deficient and -sufficient mice (95 d of age: mean tumor burden of uPARAP/Endo180^{+}/PymT^{+}, 9.2 g, range 5.2–16.8 g [n = 19 mice]; uPARAP/Endo180$^{-/-}$/PymT^{+}, 6.6 g, range 3.4–11.0 g [n = 18 mice], P < 0.0061, *t* test; P < 0.0093, Wilcoxon rank sum test. 105 d of age: uPARAP/Endo180^{+}/PymT^{+}, 15.1 g, range 6.6–26.4 g [n = 48 mice]; uPARAP/Endo180$^{-/-}$/PymT^{+}, 11.5 g, range 5.0–20.6 g [n = 41 mice], P < 0.00024, *t* test; P < 0.00065, Wilcoxon rank sum test).

In summary, the studies presented here suggest that uPARAP/Endo180-dependent intracellular collagen degradation is functionally important to mammary tumor growth.

Discussion

uPARAP/Endo180 is a collagen internalization receptor that is expressed exclusively on mesenchymal cells, and its association with human epithelial tumors stems from its consistent and dramatic overexpression by mesenchymal cells embedded within the supporting tumor stroma rather than from its expression by tumor cells (St Croix et al., 2000; Schnack Nielsen et al., 2002). In this paper, we investigated the specific functions of stromal uPARAP/Endo180 in tumorigenesis by using a validated mouse model of human ductal mammary adenocarcinoma (Maglione et al., 2001; Lin et al., 2003). Our results show that intracellular collagen degradation is a quantitatively relevant pathway for the turnover of collagen during tumor progression. The data also show that this process is mediated by uPARAP/Endo180. Tumors deprived of uPARAP/Endo180 displayed an abrogation of cellular collagen uptake, a fibrotic state characterized by the accumulation of both basement membrane and interstitial collagens, and an overall tumor size reduction, despite the collagen accumulation.

A previous study has shown that MT1-MMP–dependent pericellular collagen degradation is a critical regulator of tumor cell proliferation (Hotary et al., 2003). A direct impairment of tumor cell proliferation caused by the lack of uPARAP/Endo180-dependent intracellular collagen degradation and the associated accumulation of interstitial and basement membrane collagen, therefore, suggested a plausible explanation for the impaired tumor growth in uPARAP/Endo180-deficient mice. However, despite pronounced differences in collagen deposition, proliferation rates were similar in uPARAP/Endo180-sufficient and -deficient tumors. Furthermore, no appreciable differences were detected in the rate of apoptosis. The specific mechanism by which uPARAP/Endo180-dependent collagen turnover promotes mammary tumor progression, therefore, remains to be determined.

The extracellular/pericellular MMP-dependent pathway of collagen turnover has been extensively studied and has been the target of clinical cancer trials in humans (McCawley and Matrisian, 2000; Coussens and Werb, 2002; Mott and Werb, 2004). In contrast, the functional relevance of intracellular collagen turnover to tumor progression in vivo was essentially undefined before this study, owing largely to the inability to experimentally manipulate the process; this obstacle was overcome with the generation of uPARAP/Endo180-deficient mice (Engelholm et al., 2001a; East et al., 2003). Because of the data presented in this paper, it can now be concluded that intracellular collagen degradation is both functionally relevant to collagen turnover in cancer and also represents an important pathway of turnover of this, the most abundant of the ECM components. The expression of uPARAP/Endo180 in human cancer is still under investigation (Behrendt, 2004). It is noteworthy, however, that the receptor has been found to be expressed in the stroma of all human carcinomas investigated to date (St Croix et al., 2000; Schnack Nielsen et al., 2002). Moreover, uPARAP/Endo180 expression has been reported also at sites of nonneoplastic tissue degenerative diseases such as osteoarthritis (Howard et al., 2004), and intracellular inclusions of phagocytosed collagen have been demonstrated in mesenchymal cells associated with periodontal disease, emphysema, and rheumatoid arthritis (Cullen, 1972; Harris et al., 1977; Soames and Davies, 1977; Neurath, 1993; Lucattelli et al., 2003). Altogether, these findings imply that uPARAP/Endo180 could have a generalized role in collagen turnover during human cancer progression as well as in other chronic tissue destructive diseases and, thus, could serve as a novel therapeutic target.

The functional relationship between extracellular MMP-dependent and intracellular uPARAP/Endo180-dependent collagenolysis remains to be elucidated. Of particular importance will be to study the possible prerequisite for fibrillar collagen cleavage before its interaction with uPARAP/Endo180. The currently available evidence tentatively suggests that the cellular uptake of collagen by uPARAP/Endo180 is independent of the prior cleavage of collagen by MMPs. First, the cellular uptake of fibrillar collagen by mesenchymal cells has been reported to be insensitive to MMP inhibition (Everts et al., 1989). Second, MT1-MMP–deficient mice, which display a severe impairment of fibrillar collagen degradation, present a dramatic compensatory increase in collagen phagocytosis by mesenchymal cells (Holmbeck et al., 1999; Szabova et al., 2005). Third, preliminary studies of mice with a combined deficiency in intracellular collagen degradation (uPARAP/Endo180$^{-/-}$) and extracellular collagen degradation (Col1A1r/r or MT1-MMP$^{-/-}$) reveal a more profound collagen remodeling defect than mice with individual deficiencies (unpublished data). Together, these data suggest that extracellular and intracellular collagen degradation pathways operate at least partially independent of each other. This raises the intriguing possibility that pharmacological inhibition of MMP activity, which is aimed at preventing pathological connective tissue destruction during cancer and other degenerative diseases, may be functionally counteracted by increased uPARAP/Endo180-dependent intracellular collagen degradation. The profound increase in intracellular collagen in connective tissue cells of mice with genetic ablation of the mesenchymal collagenase MMP-14 would support this notion (Holmbeck et al., 1999).

Materials and methods

Transgenic mice

The study was performed in accordance with animal care guidelines from the National Institutes of Health. The generation of uPARAP/Endo180$^{-/-}$ mice in a mixed C57/129 background has been described previously (Engelholm et al., 2003). The mice were backcrossed for five generations to FVB/N (The Jackson Laboratory). Next, the mice were crossed with FBN/V-TgN (MMTVPyVT) 634Mu1 (PymT) mice (The Jackson Laboratory) that were predisposed to malignant mammary adenocarcinoma as a result of the mammary gland–directed expression of a PymT oncogene (Guy et al., 1992). uPARAP/Endo180$^{+/-}$/PymT^{+} and uPARAP/Endo180$^{-/-}$/PymT^{+} male mice were crossed with uPARAP/Endo180$^{+/-}$ female mice to generate study cohorts of littermate and sibling uPARAP/Endo180$^{-/-}$/PymT^{+}, uPARAP/Endo180$^{+/-}$/PymT^{+}, and uPARAP/Endo180$^{+/+}$/PymT^{+} virgin female mice that were 98.4% congenic to FVB. Mice were genotyped by PCR from ear snip biopsies at weaning as described previously (Bugge et al., 1998), and the genotype of all mice was reconfirmed at the termination of the experiment. Each mammary gland of the mice in the study cohorts was palpated weekly, beginning at weaning, for the formation of mammary tumors by an investigator who was unaware of animal genotype. Mice were killed at the termination of the experiment, and the total mammary tumor burden was determined as the cumulative weight of each tumor dissected from the mammary gland by an investigator who was unaware of animal genotype.

Tumor explant cultures and collagen internalization assays

Tumor-bearing mice were anesthetized by a brief inhalation of CO_2 and were perfused intracardially with 10 ml of ice-cold PBS. Sections of tumors (~1 mg) from the left inguinal mammary gland were aseptically removed, finely minced with a scalpel and scissors, and washed with DME/Ham's F12 (1:1; 100 U/ml penicillin and 100 U/ml streptomycin). The minced tumor tissue was incubated for 40 min at 37°C with continuous agitation in 5 ml of a solution containing 2.5 mg/ml trypsin (GIBCO BRL) and 850 U/ml of type II collagenase (GIBCO BRL) in PBS containing 5 mg/ml BSA. The enzymatic action was terminated by adding 1 vol DME/Ham's F12 containing 5% FCS. The resultant cell suspension was washed once in DME/Ham's F12 and plated on poly-D-lysine–coated glass coverslips. The mixed tumor–stromal explants were maintained in DME/Ham's F12 containing 5% FCS in a tissue culture incubator at 5% CO_2.

For collagen internalization experiments, the mixed tumor–stromal explants were incubated for 1 h with 20 μM E64d (Calbiochem) at 37°C, and 25 μg/ml of Oregon green 488 collagen IV (Molecular Probes) was added. For time course experiments, Oregon green 488 collagen IV was added for 30 min at 4°C, and unbound collagen was washed away. 50 nM LysoTracker (Molecular Probes) and DAPI were added 1 h before the end of the experiment to visualize the lysosomes and nuclei, respectively. For visualization of cytokeratin by immunofluorescence analysis, LysoTracker was omitted, and the cells were fixed at the termination of the experiment with 4% PFA in PBS for 20 min. The coverslips were blocked

with 100 mM glycine followed by 1% BSA in PBS and were incubated with cytokeratin antibodies (Abcam) followed by rhodamine-conjugated donkey anti–rabbit (1:200; Jackson ImmunoResearch Laboratories). DAPI (Vector Laboratories) was added to visualize nuclei. Confocal images were collected on a confocal system (model TCS SP2; Leica) using an upright microscope (model DM-RE-7; Leica) and a 63× 1.32 NA objective. Projection images from the resulting files were made using the LCS software (Leica).

Transmission EM

Tumor-bearing mice were perfused intracardially with ice-cold PBS. Mammary tumors were dissected into 1-mm^3 pieces and were fixed overnight in 2.5% glutaraldehyde and 2% PFA in 0.1 M sodium cacodylate buffer, pH 7.4, at 4°C. The samples were postfixed with 1% OsO_4 for 2 h in the dark, followed by dehydration and embedding. The blocks were polymerized at 68°C for 48 h. Sections were mounted on copper grids and were stained with uranyl acetate and lead citrate. The sections were then subjected to an exhaustive analysis for intracellular collagen inclusions by using a transmission electron microscope (model 1010; JEOL) operated at 80 kEV.

Histological analysis

Tumor-bearing mice were anesthetized by a brief inhalation of CO_2 and were perfused intracardially with 10 ml of ice-cold PBS, followed by 10 ml of 4% PFA in PBS (Electron Microscopy Sciences). The tumors were excised, bisected along the longest axis, and were either embedded in optimal cutting temperature and immediately frozen in liquid N_2 or were fixed for 24 h in 20 vol of 4% PFA in PBS and processed into paraffin. Immunostaining was performed with a Vectastain ABC peroxidase kit (Vector Laboratories) using DAB as the chromogenic substrate. Collagen type I telopeptides were detected with LF-67 rabbit polyclonal antiserum (Bernstein et al., 1996); collagen type I propeptides with LF-41 antibodies (Fisher et al., 1989); decorin with LF-113 rabbit anti–mouse decorin pAb (Fisher et al., 1995; all were provided by L. Fisher, National Institute of Dental and Craniofacial Research, Bethesda, MD); type IV collagen telopeptides with rabbit pAb (Abcam); nidogen with rat anti–mouse nidogen mAb (BD Biosciences); and fibronectin with rabbit pAb (Santa Cruz Biotechnology, Inc.), using 5–8-μm cryostat sections. Sections were counterstained with Mayer's hematoxylin (Zymed Laboratories). For unbiased quantitative histomorphometric analysis of collagen and fibronectin, random low magnification (10×) micrographs of tumors were collected as TIFF files. The fraction of antigen-positive pixels relative to the total field area was determined with MetaMorph version 5.0r7 software (Universal Imaging Corp.) by using the threshold image function. The threshold area corresponding to antigen-positive regions was then assessed, and the percent coverage of the total image area was calculated by using the region measurement ability in the software. All measurements were performed by an investigator who was unaware of mouse genotype. Endothelial cells were stained with rat anti–mouse CD31 (PECAM-1; BD Biosciences), and macrophages were detected with rat anti–mouse F4/80 (Caltag Laboratories) using 5–8-μm paraffin sections and procedures as described above. Quantitation of vessel and macrophage densities was performed by an investigator who was unaware of animal genotype by using an ocular grid and a 40× objective, counting 25 fields from five tumors of each genotype. For uPARAP/Endo180 immunohistochemistry, paraffin sections were proteolytically digested with proteinase K. Affinity-purified rabbit pAb against mouse uPARAP/Endo180 were incubated at 0.5 mg/ml overnight at 4°C. The next day, they were detected with Envision-Rabbit reagent (DakoCytomation), followed by signal amplification for 5 min using biotinyl tyramine (NEN Life Science Products) and streptavidin-HRP for 30 min and were incubated with NovaRed substrate for 10 min. For the determination of proliferation rates, tumor-bearing mice were injected with BrdU 2 h before they were killed, and cell proliferation was visualized by staining with BrdU antibodies. Apoptotic nuclei were visualized by TUNEL staining using an Apotag kit (Intergen) as recommended by the manufacturers. Quantification of proliferating cells and apoptotic nuclei was performed by an investigator who was unaware of animal genotype by using an ocular grid and a 40× objective, counting 10 random sections per tumor. Proliferative and apoptotic indices were determined as the fraction of BrdU-positive cells or apoptotic nuclei as a percentage of total cells in each section.

In situ hybridization

uPARAP/Endo180 in situ hybridization was performed exactly as described previously (Engelholm et al., 2001b) by using two sets of nonoverlapping sense and antisense uPARAP/Endo180 cDNA probes. MT1-MMP and MMP-13 in situ hybridization were performed essentially as described previously (Blavier et al., 2001). In brief, paraffin sections that were prepared as described above were dewaxed in xylene, rehydrated through a series of ethanol solutions of decreasing concentrations, treated with 5 μg/ml proteinase K, postfixed in 4% PFA in PBS, acetylated in triethanolamine hydrochloride/acetic anhydride, washed in PBS, dehydrated, and air dried. The sections were incubated overnight at 50°C in hybridization buffer containing a single-stranded riboprobe that was radiolabeled with ^{33}P-UTP (PerkinElmer) and complementary sense probes. For the detection of MT1-MMP mRNA, a probe containing nt 291–902 of the published MT1-MMP cDNA (GenBank/EMBL/DDBJ under accession no. X83536) was used, and for the detection of MMP-13, a probe containing nt 1236–1903 of the murine MMP-13 cDNA (GenBank/EMBL/DDBJ under accession no. X66473) was used (both were provided by L. Blavier, National Institutes of Health, Bethesda, MD). After hybridization, the sections were washed extensively, dehydrated, and air dried. The slides were then dipped in photographic emulsion (Hypercoat LM-1; Amersham Biosciences) and were exposed for 3–5 d at 4°C. After exposure, the slides were developed and counterstained with Mayer's hematoxylin.

Northern blot analysis

Tumor-bearing mice were anesthetized by a brief inhalation of CO_2 and perfused intracardially with 10 ml of ice-cold PBS. Mammary tumors were excised, snap-frozen in liquid nitrogen, and ground to a fine powder with a mortar and pestle. Total RNA was prepared by extraction in TRIzol reagent (GIBCO BRL), as recommended by the manufacturers. 10 μg of RNA samples were fractionated electrophoretically on formaldehyde agarose gels, blotted onto NytranSuperCharge nylon membranes (Schleicher & Schuell), and hybridized to PCR-generated ^{32}P-labeled murine Col1A1 (nt 3648–3879 from Genbank/EMBL/DDBJ under accession no. 007742; amplified by using the primers 5′-CGGTTATGACTTCAGCTTCCTGCC-3′ and 5′-GCTCTTCCAGTCAGAGTGGCACAT-3′), Col4A1 (nt 6002–6188 from GenBank/EMBL/DDBJ under accession no. BC072650.1; amplified using the primers 5′-GGAGCTGGGAAGTTGCCTGTGTG-3′ and 5′-ATAATGAGCCCTGTGCCTGGCGC-3′), or a full-length murine GAPDH cDNA probe. Membranes were exposed to PhosphorImage screens and hybridization signals that were quantitated with ImageQuant software (Molecular Dynamics).

Gelatin zymography and reverse zymography

Tumors were frozen in liquid nitrogen and homogenized in PBS with a Dounce homogenizer (model 1984-100-15; Bellco Biotechnology). The homogenate was centrifuged at 25,000 *g* for 30 min, and the pellet was resuspended in PBS with sonication. SDS was added to a final concentration of 1%, and the samples were mixed gently at RT for 1.5 h. The samples were spun again, and the amount of protein in the supernatants was determined by bicinchoninic acid protein assay (Pierce Chemical Co.). Equal amounts of protein were loaded onto a gelatin zymogram (Invitrogen), and the zymogram was run and developed according to the manufacturer's instructions. For reverse zymography, equal amounts of protein were loaded on 17% polyacrylamide reverse zymogram gels prepared with 2.5 mg/ml gelatin and 0.075 μg/ml gelatinase A. The zymograms were developed for 30 h at 37°C in 50 mM Tris, pH 7.4, 0.2 M NaCl, 5 mM $CaCl_2$, and 0.02% (wt/vol) Brij-35.

We thank Dr. Q.-C. Yu for expert assistance on electron microscopy, Dr. L. Blavier for cDNA probes, Dr. L. Fisher for collagen and decorin antibodies, and Dr. W. Swaim for help with confocal microscopy.We also thank Drs. R. Angerer, S. Wahl, H. Birkedal-Hansen, S. Gutkind, and M.J. Danton for critically reading the manuscript and C. Lønborg and P. Knudsen for technical assistance.

This work was supported by grants from the Department of Defense (DAMD-17-02-1-0693 to T.H. Bugge), The Weiman Foundation (to B.S. Nielsen), and the European Commission (QGL1-CY-2000-01131 to B.S. Nielsen and L.H. Engelholm).

Submitted: 29 November 2004
Accepted: 5 May 2005

References

Behrendt, N. 2004. The urokinase receptor (uPAR) and the uPAR-associated protein (uPARAP/Endo180): membrane proteins engaged in matrix turnover during tissue remodeling. *Biol. Chem.* 385:103–136.

Bernstein, E.F., Y.Q. Chen, J.B. Kopp, L. Fisher, D.B. Brown, P.J. Hahn, F.A. Robey, J. Lakkakorpi, and J. Uitto. 1996. Long-term sun exposure alters the collagen of the papillary dermis. Comparison of sun-protected and

photoaged skin by northern analysis, immunohistochemical staining, and confocal laser scanning microscopy. *J. Am. Acad. Dermatol.* 34:209–218.

Blavier, L., A. Lazaryev, J. Groffen, N. Heisterkamp, Y.A. DeClerck, and V. Kaartinen. 2001. TGF-beta3-induced palatogenesis requires matrix metalloproteinases. *Mol. Biol. Cell.* 12:1457–1466.

Bugge, T.H., L.R. Lund, K.K. Kombrinck, B.S. Nielsen, K. Holmback, A.F. Drew, M.J. Flick, D.P. Witte, K. Danø, and J.L. Degen. 1998. Reduced metastasis of Polyoma virus middle T antigen-induced mammary cancer in plasminogen-deficient mice. *Oncogene.* 16:3097–3104.

Chambers, A.F., A.C. Groom, and I.C. MacDonald. 2002. Dissemination and growth of cancer cells in metastatic sites. *Nat. Rev. Cancer.* 2:563–572.

Coussens, L.M., and Z. Werb. 2002. Inflammation and cancer. *Nature.* 420: 860–867.

Cullen, J.C. 1972. Intracellular collagen in experimental arthritis in rats. *J. Bone Joint Surg. Br.* 54:351–359.

Danø, K., P.A. Andreasen, J. Grondahl-Hansen, P. Kristensen, L.S. Nielsen, and L. Skriver. 1985. Plasminogen activators, tissue degradation, and cancer. *Adv. Cancer Res.* 44:139–266.

Danø, K., J. Romer, B.S. Nielsen, S. Bjorn, C. Pyke, J. Rygaard, and L.R. Lund. 1999. Cancer invasion and tissue remodeling — cooperation of protease systems and cell types. *APMIS.* 107:120–127.

Dran, G., I.A. Luthy, A.A. Molinolo, F. Montecchia, E.H. Charreau, C.D. Pasqualini, and C. Lanari. 1995. Effect of medroxyprogesterone acetate (MPA) and serum factors on cell proliferation in primary cultures of an MPA-induced mammary adenocarcinoma. *Breast Cancer Res. Treat.* 35:173–186.

East, L., A. McCarthy, D. Wienke, J. Sturge, A. Ashworth, and C.M. Isacke. 2003. A targeted deletion in the endocytic receptor gene Endo180 results in a defect in collagen uptake. *EMBO Rep.* 4:710–716.

Engelholm, L.H., B.S. Nielsen, K. Danø, and N. Behrendt. 2001a. The urokinase receptor associated protein (uPARAP/endo180): a novel internalization receptor connected to the plasminogen activation system. *Trends Cardiovasc. Med.* 11:7–13.

Engelholm, L.H., B.S. Nielsen, S. Netzel-Arnett, H. Solberg, X.D. Chen, J.M. Lopez Garcia, C. Lopez-Otin, M.F. Young, H. Birkedal-Hansen, K. Danø, et al. 2001b. The urokinase plasminogen activator receptor-associated protein/endo180 is coexpressed with its interaction partners urokinase plasminogen activator receptor and matrix metalloprotease-13 during osteogenesis. *Lab. Invest.* 81:1403–1414.

Engelholm, L.H., K. List, S. Netzel-Arnett, E. Cukierman, D.J. Mitola, H. Aaronson, L. Kjøller, J.K. Larsen, K.M. Yamada, D.K. Strickland, et al. 2003. uPARAP/Endo180 is essential for cellular uptake of collagen and promotes fibroblast collagen adhesion. *J. Cell Biol.* 160:1009–1015.

Everts, V., R.M. Hembry, J.J. Reynolds, and W. Beertsen. 1989. Metalloproteinases are not involved in the phagocytosis of collagen fibrils by fibroblasts. *Matrix.* 9:266–276.

Everts, V., E. van der Zee, L. Creemers, and W. Beertsen. 1996. Phagocytosis and intracellular digestion of collagen, its role in turnover and remodelling. *Histochem. J.* 28:229–245.

Fisher, L.W., W. Lindner, M.F. Young, and J.D. Termine. 1989. Synthetic peptide antisera: their production and use in the cloning of matrix proteins. *Connect. Tissue Res.* 21:43–48; discussion 49–50.

Fisher, L.W., J.T. Stubbs III, and M.F. Young. 1995. Antisera and cDNA probes to human and certain animal model bone matrix noncollagenous proteins. *Acta. Orthop. Scand. Suppl.* 266:61–65.

Gelb, B.D., G.P. Shi, H.A. Chapman, and R.J. Desnick. 1996. Pycnodysostosis, a lysosomal disease caused by cathepsin K deficiency. *Science.* 273:1236–1238.

Guy, C.T., R.D. Cardiff, and W.J. Muller. 1992. Induction of mammary tumors by expression of polyomavirus middle T oncogene: a transgenic mouse model for metastatic disease. *Mol. Cell. Biol.* 12:954–961.

Hanahan, D., and R.A. Weinberg. 2000. The hallmarks of cancer. *Cell.* 100:57–70.

Harris, E.D., Jr., A.M. Glauert, and A.H. Murley. 1977. Intracellular collagen fibers at the pannus-cartilage junction in rheumatoid arthritis. *Arthritis Rheum.* 20:657–665.

Holmbeck, K., P. Bianco, J. Caterina, S. Yamada, M. Kromer, S.A. Kuznetsov, M. Mankani, P.G. Robey, A.R. Poole, I. Pidoux, et al. 1999. MT1-MMP-deficient mice develop dwarfism, osteopenia, arthritis, and connective tissue disease due to inadequate collagen turnover. *Cell.* 99:81–92.

Hotary, K.B., E.D. Allen, P.C. Brooks, N.S. Datta, M.W. Long, and S.J. Weiss. 2003. Membrane type I matrix metalloproteinase usurps tumor growth control imposed by the three-dimensional extracellular matrix. *Cell.* 114:33–45.

Howard, M.J., M.G. Chambers, R.M. Mason, and C.M. Isacke. 2004. Distribution of Endo180 receptor and ligand in developing articular cartilage. *Osteoarthritis Cartilage.* 12:74–82.

Kjøller, L., L.H. Engelholm, M. Hoyer-Hansen, K. Danø, T.H. Bugge, and N. Behrendt. 2004. uPARAP/endo180 directs lysosomal delivery and degradation of collagen IV. *Exp. Cell Res.* 293:106–116.

Lanari, C., I. Luthy, C.A. Lamb, V. Fabris, E. Pagano, L.A. Helguero, N. Sanjuan, S. Merani, and A.A. Molinolo. 2001. Five novel hormone-responsive cell lines derived from murine mammary ductal carcinomas: in vivo and in vitro effects of estrogens and progestins. *Cancer Res.* 61:293–302.

Lin, E.Y., J.G. Jones, P. Li, L. Zhu, K.D. Whitney, W.J. Muller, and J.W. Pollard. 2003. Progression to malignancy in the polyoma middle T oncoprotein mouse breast cancer model provides a reliable model for human diseases. *Am. J. Pathol.* 163:2113–2126.

Liotta, L.A., and E.C. Kohn. 2001. The microenvironment of the tumour-host interface. *Nature.* 411:375–379.

Liotta, L.A., K. Tryggvason, S. Garbisa, I. Hart, C.M. Foltz, and S. Shafie. 1980. Metastatic potential correlates with enzymatic degradation of basement membrane collagen. *Nature.* 284:67–68.

Liotta, L.A., P.S. Steeg, and W.G. Stetler-Stevenson. 1991. Cancer metastasis and angiogenesis: an imbalance of positive and negative regulation. *Cell.* 64:327–336.

Lucattelli, M., E. Cavarra, M.M. de Santi, T.D. Tetley, P.A. Martorana, and G. Lungarella. 2003. Collagen phagocytosis by lung alveolar macrophages in animal models of emphysema. *Eur. Respir. J.* 22:728–734.

Maglione, J.E., D. Moghanaki, L.J. Young, C.K. Manner, L.G. Ellies, S.O. Joseph, B. Nicholson, R.D. Cardiff, and C.L. MacLeod. 2001. Transgenic Polyoma middle-T mice model premalignant mammary disease. *Cancer Res.* 61:8298–8305.

McCawley, L.J., and L.M. Matrisian. 2000. Matrix metalloproteinases: multifunctional contributors to tumor progression. *Mol. Med. Today.* 6:149–156.

Mott, J.D., and Z. Werb. 2004. Regulation of matrix biology by matrix metalloproteinases. *Curr. Opin. Cell Biol.* 16:558–564.

Neurath, M.F. 1993. Detection of Luse bodies, spiralled collagen, dysplastic collagen, and intracellular collagen in rheumatoid connective tissues: an electron microscopic study. *Ann. Rheum. Dis.* 52:278–284.

Pandis, N., S. Heim, G. Bardi, J. Limon, N. Mandahl, and F. Mitelman. 1992. Improved technique for short-term culture and cytogenetic analysis of human breast cancer. *Genes Chromosomes Cancer.* 5:14–20. (published erratum appears in *Genes Chromosones Cancer*. 1992. 5:410)

Saftig, P., E. Hunziker, O. Wehmeyer, S. Jones, A. Boyde, W. Rommerskirch, J.D. Moritz, P. Schu, and K. von Figura. 1998. Impaired osteoclastic bone resorption leads to osteopetrosis in cathepsin-K-deficient mice. *Proc. Natl. Acad. Sci. USA.* 95:13453–13458.

Schnack Nielsen, B., F. Rank, L.H. Engelholm, A. Holm, K. Danø, and N. Behrendt. 2002. Urokinase receptor-associated protein (uPARAP) is expressed in connection with malignant as well as benign lesions of the human breast and occurs in specific populations of stromal cells. *Int. J. Cancer.* 98:656–664.

Sheikh, H., H. Yarwood, A. Ashworth, and C.M. Isacke. 2000. Endo180, an endocytic recycling glycoprotein related to the macrophage mannose receptor is expressed on fibroblasts, endothelial cells and macrophages and functions as a lectin receptor. *J. Cell Sci.* 113:1021–1032.

Soames, J.V., and R.M. Davies. 1977. Intracellular collagen fibrils in early gingivitis in the beagle dog. *J. Periodontal Res.* 12:378–386.

St Croix, B., C. Rago, V. Velculescu, G. Traverso, K.E. Romans, E. Montgomery, A. Lal, G.J. Riggins, C. Lengauer, B. Vogelstein, and K.W. Kinzler. 2000. Genes expressed in human tumor endothelium. *Science.* 289:1197–1202.

Szabova, L., S.S. Yamada, H. Birkedal-Hansen, and K. Holmbeck. 2005. Expression pattern of four membrane-type matrix metalloproteinases in the normal and diseased mouse mammary gland. *J. Cell. Physiol.* 10.1002/jcp.20385.

van der Rest, M., and R. Garrone. 1991. Collagen family of proteins. *FASEB J.* 5:2814–2823.

Werb, Z., T.H. Vu, J.L. Rinkenberger, and L.M. Coussens. 1999. Matrix-degrading proteases and angiogenesis during development and tumor formation. *APMIS.* 107:11–18.